Optimization of geometrical design of nested conical Wolter-I X-ray telescope

Baozhong Mu (穆宝忠)*, Hongying Liu (刘宏颖), Huijun Jin (金慧俊), Xiajun Yang (杨夏军), Fangfang Wang (王芳芳), Wenbin Li (李文彬), Hong Chen (陈 鸿), and Zhanshan Wang (王占山)

Institute of Precision Optical Engineering, Physics Department, Tongji University, Shanghai 200092, China

**Corresponding author: mubz@tongji.edu.cn*

Received February 8, 2012; accepted April 13, 2012; posted online August 3, 2012

Optical design of nested conical Wolter I X-ray telescope covering energy band from 1 to 30 keV is investigated systematically. Recurrence relation of the nested structure is deduced, and the impact of the initial parameters on the performance is analyzed. Due to the need for hard X-ray astronomical observations in China, the initial structure is presented, for which six groups of W/B_4C aperiodic multilayer coatings between the innermost and the outermost shell of the mirror are designed. The effective area, resolution, and field of view are calculated in the simulation. The results show that the effective area can achieve 71 cm^2 and the field of view can achieve $13'$ at 30 keV. The resolution is estimated to be $\sim 10''$ in half-power diameter.

OCIS codes: 340.7440, 340.7460.

doi: 10.3788/COL201210.103401.

The cosmic X-Ray background (CXB) resides in the 0.1 to 100 keV energy range. Deep X-ray surveys have resolved CXB around 1 keV into a population of discrete sources nearly entirely composed of active galactic nuclei (AGN)[1]. In addition, CXB in the 2 to 10 keV range has been completely resolved by Chandra and XMM-Newton telescopes when the sky flux is dominated by extragalactic emission. The main contributors are thought to be absorbed and unabsorbed AGNs with a mixture of quasars and narrow emission line galaxies[2,3]. The Chandra telescope, which is composed of four nested Wolter-I mirror pairs coated with a single iridium layer, could achieve the effective area of 800/400 cm[2] at 0.25/5 keV and resolution of $0.5''$[4,5]. The XMM-Newton telescope, which consists of 58 gold-coated nested Wolter-I mirrors, could achieve the effective area of 1 475/580 cm^2 at 1.5/8 keV and resolution of $16''$[6]. Many X-ray sources above 10 keV are available, such as the peak of CXB at $\sim$ 30 keV[7], which cannot be observed by currently in-orbit telescopes due to the severe decline in the effective area caused by low reflectivity of the single metal layer beyond the total external reflection. Aperiodic multilayer mirrors are preferred for high throughput in next-generation hard X-ray telescopes[8,9]. Hard X-ray telescopes are being developed, including IXO and Astro-H. IXO uses the nested Wolter-I structure with aperiodic tungsten and silicon multilayer coating. By using aperiodic multilayer coating, IXO is able to achieve an effective area of 0.6 m^2/150 cm^2 at 6/30 keV and resolution of $5''$[10,11]. To reduce the cost and the difficulty in fabrication of highly aspherical mirrors, conical structure is suggested instead of Wolter-I structure in Astro-H. Astro-H, with its coating of aperiodic platinum and carbon multilayer, is able to achieve the effective area of 300 cm^2 at 30 keV and resolution of $1.7'$[12].

Conical structures, which utilize conical mirrors instead of parabolic and hyperbolic mirrors, cannot image perfectly[13], but only at a lower resolution of a few arcsec. Actually, resolution at the arcmin level is affected by the mirror fabrication that uses the epoxy replication method. The ASCA[14], Astro-E[15], and Astro-H[12] programs, which all adopt the nested conical structure, produce high effective areas, but result in a loss of resolution. The optical design of nested conical system has not been discussed in detail. The purpose of this article is to present a detailed theoretical and computational analysis of the optical design. Based on the requirements of X-ray surveys in China, the optical design process of a nested conical Wolter-I X-ray telescope of 1 to 30 keV energy is established. The recurrence relation of the nested structure is deduced, the principle of selecting initial parameters is proposed, and corresponding aperiodic multilayer mirror is discussed.

In 1952, Wolter demonstrated a type of optics in which a paraboloid and hyperboloid combination was mounted in a coaxial and confocal arrangement. X-rays utilized two successive reflections from the paraboloid and then the hyperboloid to focus the image[16]. To overcome the difficulty in the fabrication of highly aspherical mirrors, conical mirrors were suggested in lieu of precisely curved paraboloidal and hyperboloidal surfaces. Parallel incident X-rays could not focus the image, but formed a blurred circle[13].

The diagram of the nested conical Wolter-I X-ray telescope is shown in Fig. 1. A rectangular coordinate system with origin O, ordinate r, and abscissa Z along the opposite direction of incident lights was established. X-ray incidents along the -Z direction are then reflected twice along two groups of rotating cone to focus on origin O. Here, f is the focal length from the center of secondary mirror to the focal point, t is the thickness of the mirrors, $L_{\rm P}$ is the length of primary mirror, $L_{\rm h}$ is the length of secondary mirror, and θ_N is the grazing incident angle of the Nth mirror. The primary and secondary mirrors have the same grazing incident angle. Here, r_N is the radius of the Nth secondary mirror's end point and R_N is the radius of the Nth secondary mirror's

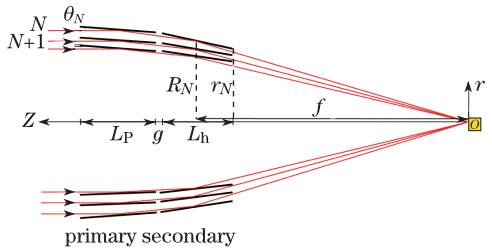

Fig. 1. Schematic of nested conical Wolter-I structure.

midpoint. Figure 1 shows the two-stage conical optics. Parallel X-ray beams are reflected twice by the conical mirror shells in two stages to converge at a focal point. In the conical structure with double reflections, the grazing incident angle θ of a mirror shell at a radius of R_N is determined by the focal length f as[15]

$$\tan(4\theta_N) = \frac{R_N}{f}. \tag{1}$$

In order to increase the geometrical area to its maximum, the inner surfaces should be sufficiently small to pass all the axial rays that strike the next outer surface[17] where the rays striking the front point of the secondary mirror are reflected furthest from the next outer secondary mirror. The recurrence relations between two adjacent shells of the mirrors can be derived as Eq. (2), where Δr_N is the vertical interval in the end point of the secondary mirror between the Nth and the $(N+1)$th shell of the mirrors. Then, the radius of the $(N+1)$th shell of mirror can be obtained by Eq. (3). In addition, the primary rays passing through each layer of the mirror are focused on the same point, O. With this requirement, the grazing incidence angle of the $(N+1)$th shell of the mirror can be deduced by r_{N+1} as

$$\Delta r_N = \tan(4\theta_N) \cdot L_\mathrm{h} - \tan(3\theta_N) \cdot L_\mathrm{h} + t, \tag{2}$$

$$r_{N+1} = r_N - \Delta r_N, \tag{3}$$

$$r_{N+1} = f \cdot \tan(4\theta_{N+1}) - \frac{L_\mathrm{h}}{2} \cdot \tan(3\theta_{N+1}). \tag{4}$$

Equations (1)–(4) indicate that the radius and grazing incident angle of inner surfaces can be calculated shell-by-shell with a specific outermost radius R_out and focal length f. With certain innermost radius R_in, the nested shells can be restricted.

The effective area and the resolution are the key performance indicators of the X-ray telescope. The total geometrical area can be expressed by

$$A = \sum_{N=1}^{n} 2\pi \cdot r_N \cdot L_\mathrm{P} \cdot \tan\theta_N. \tag{5}$$

The angle radius of spot diagram imaged by the ray incident to the Nth mirror can be expressed by

$$\theta_\mathrm{spot} = a\tan\frac{r_N - (f - \frac{L_\mathrm{h}}{2}) \cdot \tan(4\theta_N)}{f}. \tag{6}$$

Equations (2)–(6) indicate that the effective area and the resolution are decided by the focal length f, the radii R_out and R_in, the mirror lengths L_P and L_h, and the mirror thickness t. The choice of initial parameters depends on their influence on the performance and the laboratory conditions.

According to the mandrel in our laboratory, the outermost radius R_out was set as 85 mm and the innermost radius was set as 30 mm. The focal length was chosen as 4 m considering the volume and the weight of satellite that can now be provided. The remaining parameters of mirror thickness and mirror length were discussed, as shown in Figs. 2 and 3. The length of the primary mirror L_P and the length of the secondary mirror L_h can be calculated by

$$L_\mathrm{h} = \frac{L_\mathrm{P} \cdot \cos 3\theta_N}{\cos\theta_N}, \tag{7}$$

for all axial rays incident to the primary mirror that are received by the secondary mirror. Thus, only L_P needs to be discussed.

Figure 2 shows the effects of mirror thickness on the geometrical area and the resolution with L_P of 100 mm. The geometrical area decreases from 143 to 99 cm^2, whereas the resolution expressed by the half-power diameter (HPD) does not change with the increase of mirror thickness from 150 to 390 μm. Less thickness of the mirrors is a crucial factor to obtain a larger effective area. Mirrors with thicknesses of 400 and 200 μm were available in our laboratory; therefore, mirrors of 200-μm thickness were chosen.

Figure 3 shows the effects of mirror length on the geometrical area and the resolution with the mirror of 200-μm thickness. The resolution decreases from 9″ to 26″, whereas the geometrical area increases from 131 to 173 cm^2 with increased mirror length from 100 to 300 mm.

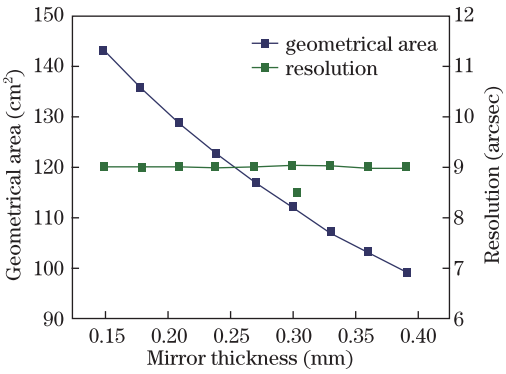

Fig. 2. Performance with different mirror thicknesses.

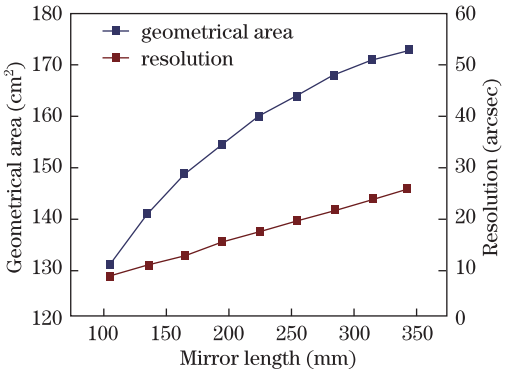

Fig. 3. Performance with different mirror lengths.

The enlargement of the geometrical area by lengthening mirror results in a loss of resolution. Therefore, the choice of mirror length must balance the geometrical area and the resolution, and must also rely on the actual engineering. A large geometrical area can be obtained by thinner mirrors; therefore, we chose the mirror length of 100 mm to meet the resolution and the requirements of the system.

With this group of parameters, the initial structure could be determined. In the nested structure were 101 shells of mirrors. From outer to inner, the interval between two adjacent shells gradually decreased. The interval between the first and the second shells of the mirrors was 0.7313 mm; however, between the 100th and the 101th shells of mirrors, the interval was 0.3908 mm. The change of grazing incident angle between two adjacent shells of mirrors was also gradually decreased from 0.0026° to 0.0014°.

The effective area can be described as the product of total geometrical area and mirror's reflectivity:

$$A_{\text{eff}} = \sum_{N=1}^{n} 2\pi \cdot r_N \cdot L_{\text{P}} \cdot \tan\theta_N \cdot R(E, \theta_N), \qquad (8)$$

where $R(E,\ \theta_N)$ is the reflectivity of the multilayer coating related to the X-ray energy and the grazing incident angles. Clearly, the high reflectivity R becomes the key point if a large effective area of the X-ray telescope is pursued. For X-ray observation, mirror surfaces should be coated by a single metal layers or multiple layers in order to enhance reflectivity[5,12]. A single metal layer is adequate for early X-ray observations below 10 keV[5]. However, because the scientific objectives extend to the hard X-ray region, the single metal layer does not have sufficient reflectivity above 10 keV when the grazing incident angle becomes relatively high. As shown in Fig. 4, the Au single layer has nearly no reflectivity in the hard X-ray region above 15 keV when the grazing incident angle is 0.3°. Compared with single layer and periodic multilayer coating, the aperiodic multilayer coating has high throughput in hard X-ray region and high reflectivity in a wide energy band. Thus, an aperiodic multilayer coating is preferred for the 1 to 30 keV X-ray surveys.

The flatness of reflectivity curve and integrated reflectivity are of concern with regard to multilayer coatings.

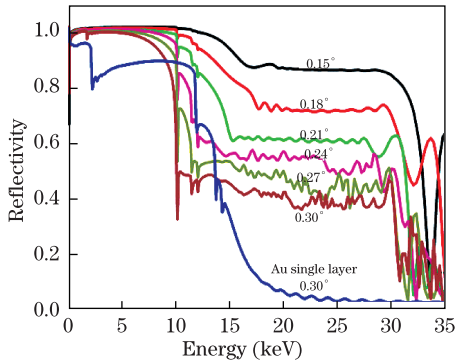

Fig. 4. Reflectivity curves of six groups aperiodic multilayer coatings. The values above each curve indicate the incident angle for each aperiodic multilayer coating, whereas the angle regions used for each group of aperiodic multilayer coating are 0.1° to 0.15°, 0.15° to 0.18°, 0.1° to 0.21°, 0.21° to 0.24°, 0.24° to 0.27°, and 0.27° to 0.30°, respectively.

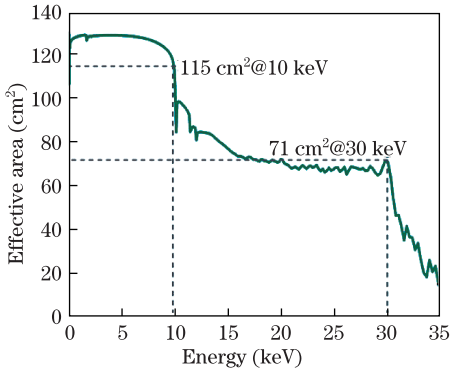

Fig. 5. Change of effective area as X-ray energy changes.

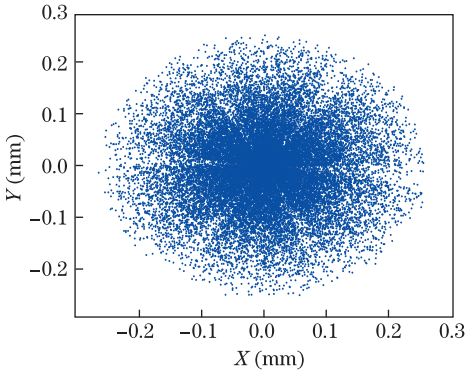

Fig. 6. Spot diagram in the focal plane.

However, for wide-band aperiodic multilayer coating, too large region of grazing incident angle will cause reflectivity to become drastically reduced, even to zero. According to Eq. (1), an aperiodic multilayer coating was designed for use in the grazing incidence angle region of 0.1° and 0.3°[18]. W/B_4C combination was selected as the layer materials, which has been confirmed to have good performance up to 70 keV. The grazing incident angle of 0.1° to 0.3° was divided into six groups and optimized for each group, as shown in Fig. 4. For all the mirror groups, the interfacial roughness between W and B_4C was set to be 0.45 nm. Figure 4 shows that the reflectivity of the first group, for which the grazing incident angle is 0.15°, features an excellent uniformity and average reflectivity of above 80% in energy region of 1 to 30 keV. When the grazing incidence angle was increased, the reflectivity of the following groups decreased from 65% to 37%. Mirrors in the same group were coated with an identical multilayer design.

By using the initial structure mentioned above, the performance simulation would give the effective area, the resolution and the field of view. In Fig. 5, the effective area is plotted against X-ray energy from 1 to 30 keV. The figure shows that effective areas of 115 and 71 cm^2 were achieved at 10 and 30 keV, respectively.

The image quality and the resolution were evaluated by the spot diagram, as shown in Figs. 6 and 7. The blank sectors in the spot diagram were caused by the support structure of mirrors. The angular resolution was calculated to be 10″ in HPD, with no consideration of tolerance.

The nested conical Wolter-I structure features a constant spatial resolution across the field of view. The field

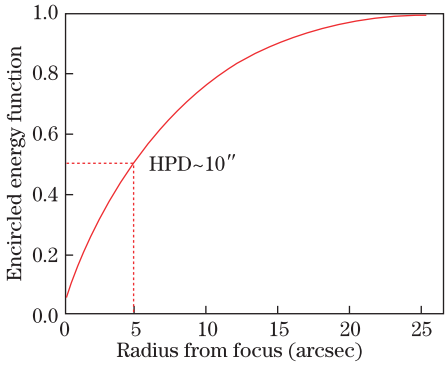

Fig. 7. Encircled energy of the spot diagram.

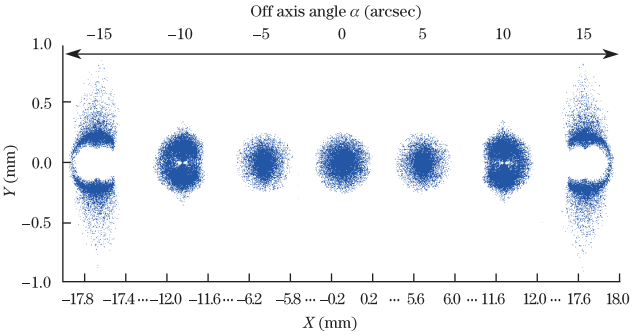

Fig. 8. Changes in the spot diagram as the off-axis angle changes.

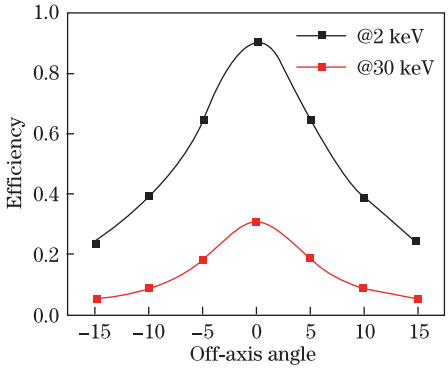

Fig. 9. Change in efficiency as the off-axis angle changes.

of view was defined as the off-axis angle α, at which the effective area decreased to one half of its on-axis value[12]. Figure 8 shows the changes of spot diagram in the focal plane as the off-axis angles changed. With the off-axis angle α changed, the spot diagram shifted to both sides of the original. The X width of spot diagram did not change within 0.4 mm, whereas the Y width increased from 0.4 to 2 mm. Statistics of the effective efficiency as off-axis angles changed at 2 and 30 keV was shown in Fig. 9. The field of view was achieved as $16'/13'$ at 2/30 keV, respectively.

In conclusion, the optical design of nested conical Wolter-I X-ray telescope is investigated. The radius and grazing incident angle of inner surfaces can be calculated shell-by-shell with specific outermost radius and focal length. The mirror length and the mirror thickness are determined through their impact on the geometrical area and the resolution. With focal length of 4 m, outermost radius of 85 mm, mirror length of 100 mm, and mirror thickness of 200 μm, 101 shells of mirrors are constructed. For the energy region of 1 eV to 30 keV, a W/B_4C aperiodic multilayer mirror is suggested and designed. The effective area and the field of view are simulated to be 71 cm^2 and $13'$ at 30 keV, and the resolution was estimated to be $10''$ with no consideration of tolerance. The effects of tolerance, including figure error, alignment error, and other possible errors, will be discussed in our next work, which can provide basis for the replication of mirrors and alignment of the system.

This work was supported by the National Natural Science Foundation of China (Nos. 10978002, 11027507, and 10825521), the National International Cooperation Program between China and Japan (No. 2008DFA01920), the Shanghai Science and Technology Development Fund (No.10QA1406900.), and the New Century Excellent Talents in University.

References

1. C. Budtz-Jørgensen, T. Takahashi, L. Piro, I. Kuvvetli, A. Holland, D. Lumb, and P. de Kortef, Proc. SPIE **5165,** 37 (2004).
2. R. Gilli, Adv. Space Res. **34,** 2470 (2004).
3. W. N. Brandt and G. Hasinger, Annu. Rev. Astron. Astrophys. **43,** 827 (2005).
4. M. C. Weisskopf, S. L. O'Dell, R. F. Eisner, and L. P. van Speybroeck, Proc. SPIE **2515,** 312 (1995).
5. M. C. Weisskopf, H. D. Tananbaum, L. P. Van Speybroeck, and S. L. O'Dell, Proc. SPIE **4012,** 1 (2000).
6. D. de Chambure, R. Laine, and K. van Katwijk, Proc. SPIE **3444,** 313 (1998).
7. D. Stern Daniel, F. Harrison, D. Ballantyne, G. Madejski, and NuSTAR Team, in *Proceedings of the 213th Meeting of American Astronomical Society* 348 (2009).
8. K. Tamur, K. Yamashita, and Y. Tawara, Proc. SPIE **4138,** 111 (2000).
9. F. Wang, W. Li, Q. Huang, J. Zhu, B. Mu, and Z. Wang, Chin. Opt. Lett. **9,** 091601(2011).
10. R. S. McClelland and D. W. Robinson, in *Proceedings of IEEE Conference on Aerospace* 1 (2009).
11. J. Bookbinder, Proc. SPIE **7732,** 77321B (2010).
12. T. Takahashi, T. K. Mitsuda, and R. Kelley, Proc. SPIE **7732,** 77320Z (2010).
13. R. Petre and P. J. Serlemitsos, Appl. Opt. **24,** 1833 (1985).
14. Y. Tsusaka, H. Suzuki, and K. Yamashita, Appl. Opt. **34,** 4848 (1995).
15. H. Kunieda, M. Ishida, and T. Endo, Appl. Opt. **40,** 553 (2001).
16. V. H. Wolter, Ann. Phys. **10,** 94 (1952).
17. L. P. van Speybroeck and R. C. Chase, Appl. Opt. **11,** 440 (1972).
18. F. Wang, J. Zhu, M. Tan, L. Jiang, and Z. Wang, Proc. SPIE **7995,** 1 (2011).